Applied Catalysis A: General 350 (2008) 237–243

Contents lists available at ScienceDirect

Applied Catalysis A: General

journal homepage: www.elsevier.com/locate/apcata

Structural and photocatalytic degradation characteristics of hydrothermally treated mesoporous TiO_2

Taicheng An [a,*], Jikai Liu [a,c], Guiying Li [a], Shanqing Zhang [b], Huijun Zhao [b,**], Xiangying Zeng [a], Guoying Sheng [a], Jiamo Fu [a]

[a] State Key Laboratory of Organic Geochemistry and Guangdong Key Laboratory of Environmental Resources Utilization and Protection, Guangzhou Institute of Geochemistry, Chinese Academy of Sciences, Guangzhou 510640, China
[b] Australian Rivers Institute and Griffith School of Environment, Gold Coast Campus, Griffith University, Qld 4222, Australia
[c] Graduate School of Chinese Academy of Sciences, Beijing 100049, China

ARTICLE INFO

Article history:
Received 10 June 2008
Received in revised form 14 August 2008
Accepted 23 August 2008
Available online 29 August 2008

Keywords:
Mesoporous TiO_2
Texture control
PEG template
Photocatalytic activity
Tribromophenol

ABSTRACT

Mesoporous TiO_2 photocatalysts have been synthesized using polyethylene glycol (PEG) as a template direction agent in diluted acetic acid aqueous solution. This medium slows down the hydrolysis reaction of titanium sources due to the hydrolytic retardant and the strong chelating effects of acetic acid. A hydrothermal treatment process was introduced to better control the resultant mesoporous structures. The effects of PEG molecular weight and thermal treatment temperature on the resultant structure and photoactivity were investigated. Morphological, structural and phase compositional properties of the resultant photocatalysts were systematically characterized using transmission electron microscopy, X-ray diffraction and nitrogen adsorption/desorption analysis. The mesoporous structure with diameters between 13.3 and 17.0 nm and mean porous sizes that ranged from 9.6 to 13.3 nm were obtained when the molecular weight of PEG were varied from 200 to 20,000. The mesoporous diameters were changed significantly from 9.8 to 18.4 nm with mean porous sizes slightly increasing from 8.0 to 10.0 nm when the calcination temperature was varied from 350 to 550 °C. The activities of the resultant TiO_2 photocatalysts were evaluated using 2,4,6-tribrominated phenol as a testing compound that represents a class of toxic brominated flame retardants. The experimental results revealed that the photocatalytic activity depends on the phase and on the structural characteristics of the resultant photocatalysts.

1. Introduction

Synthesis of mesoporous metal oxide functional materials, especially mesoporous titanium dioxide, has been a hot topic of interest to researchers in many different fields, due to enormous application potentials of such materials as membranes, in catalysis and solar energy conversion and as chemical sensors [1–8]. This class of materials possesses well-defined porous sizes, porosity and large specific surface areas [9,10]. When they are used as catalysts for photocatalytic degradation of organics, these desirable properties are anticipated to improve the photocatalytic activity because the performances of such photocatalysts rely on these attributes [3,4,7,9,10]. During the past two decades, many synthetic methods have been proposed to obtain mesoporous titanium dioxide (M-TiO_2), including sol–gel method, template method, hydrothermal method, solvothermal method, ultrasound-induced method, ion liquid method, and evaporation-induced self-assembly method [11–18]. Among these methods, the sol–gel method is probably the simplest method, but formation of aggregated nanoparticles during the precipitation and post-calcination processes often lead to poorly defined mesoporous structures [19].

In order to obtain well-defined mesoporous structures and better control on porous size and porosity of the resultant material, various structural directing reagents have been introduced to sol–gel processes. These structural directing reagents are capable of forming long-ranged 3D nanosize networks, which can be used as structural templates to define a mesoporous structure [6,20–23]. To date, well-defined M-TiO_2 with mean pore sizes below 10 nm have been successfully synthesized by employing different structural directing reagents [6,14,19,21,24]. Nevertheless, the synthesis of large-pores M-TiO_2 remains as a challenge due to the rapid hydrolysis of titanium precursors that is difficult to control. In practice, strong acids (i.e. HCl and HNO_3) and complex reagents

* Corresponding author. Tel.: +86 20 85291501; fax: +86 20 85290706.
** Corresponding author. Tel.: +61 7 55528261; fax: +61 7 55528067.
E-mail addresses: antc99@gig.ac.cn (T. An), h.Zhao@griffith.edu.au (H. Zhao).

0926-860X/$ – see front matter © 2008 Elsevier B.V. All rights reserved.
doi:10.1016/j.apcata.2008.08.022

(i.e. acetylacetone, oxalate, citrate) are commonly employed to reduce the rapidity of the hydrolysis process [25,26]. When a strong acid is employed, the pH of the reaction solution changes rapidly with time, which may lead to formation of less porous and larger particle-sized TiO_2 [27]. Recently, a weak acid such as acetic acid (HAc) has been used to replace strong acids for better control of the hydrolysis process of titanium sources due to the chelating effect of acetic anions and formation of pH buffer [14,27].

Polyethylene glycol (PEG) has been frequently used as a structure-directing reagent to obtain nanoporous SiO_2 [9,24,28], aluminosilicate [29,30] and other composite materials [17]. However, only a limited number of investigations has been targeted to produce M-TiO_2 by employing PEG as the structural directing reagent [6,10,31,32]. In this work, we report a new synthesis procedure that can be used to produce large pore-sized M-TiO_2. The new procedure employs PEG and acetic acid as the structural directing reagent and hydrolytic retardants, respectively. The new procedure also involves a post hydrothermal treatment process to improve the quality of the resultant M-TiO_2. The effect of synthesis conditions on the structural characteristics of the resultant M-TiO_2 was investigated. The photocatalytic degradation of 2,4,6-tribromophenol (TBP) was conducted to demonstrate the photocatalytic performance of the resultant M-TiO_2. TBP represents a widely used brominated flame retardant materials that has been widely used as a flame retardant to reduce fire risk for production of electronic devices, epoxy, polyurethane, plastics, paper, textiles and as a synthetic intermediate for production of commercial brominated flame retardants (BFRs) and fire extinguishing media [33]. TBP is also used for production of pesticides and wood preservatives. It has been reported that toxic intermediates, such as brominated benzenes and brominated diphenyl esters, can be formed during the biodegradation of TBP [34]. Moreover, TBP can also be frequently detected in food [35], solids and sawdust [36] as well as water bodies [37]. The material is believed to be toxic to aquatic organisms and may have long-term adverse impacts on the aquatic environment, as well as posing possible risks to the human foetus. Therefore, development of an effective mean to remove TBP from the contaminated matrix is of practical importance for maintaining a healthy environment.

2. Experimental

2.1. Preparation of M-TiO_2

M-TiO_2 was prepared using the hydrothermal-assistant sol–gel method. In a typical synthesis procedure, 5 g of titanium butoxide (M = 340.36, 98%, $Ti(OC_4H_9)_4$) was added drop-by-drop to 30 mL of HAc (A.R.) aqueous solution (20%, v/v) under vigorous stirring. The mixed solution was sealed and stirring was continued for 4 h to obtain solution A. In a separate beaker, 3 g of PEG (A.R.) with the molecular weight of 600 (designated as PEG600) was dissolved in 20 mL ethanol (A.R.) under vigorous stirring to obtain solution B. Solution B was then added drop-by-drop to solution A. The final mixed solution was sealed and stirred for 24 h at room temperature. The resultant solution was then transferred into a Teflon sealed container for hydrothermal treatment under a constant temperature of 120 °C for 48 h. The precipitations were then collected and dried overnight in air at 80 °C. The as-prepared sample was then subjected to a thermal treatment process at 450 °C for 4 h. To investigate the effect of hydrothermal treatment, we replaced the 48 h hydrothermal treatment process by a 48 h room temperature treatment process to examine the effect of calcination temperature. The as-prepared samples were calcined at 350, 450, 550 and 650 °C, respectively. Furthermore, in order to evaluate the effect of the molecular weight of PEG, we replaced the PEG600 by PEG200, PEG1000, PEG2000 and PEG20000, respectively. Deionized and doubly distilled water was used throughout the experiment.

2.2. Characterization of M-TiO_2

The crystal phase composition and crystallinity of the obtained M-TiO_2 was determined by X-ray diffractometry (XRD, Rigaku D/MAX-2200 VPC) with Cu Kα radiation (λ = 0.15418 nm) at an accelerating voltage of 40 kV, an emission current of 30 mA, and a scanning speed of 5°/min. The morphology was studied using transmission electron microscopy (TEM, JEM-2010 HR) with an accelerating voltage of 200 kV. Nitrogen adsorption and desorption isotherms were obtained at 77 K with a Micromeritics ASAP 2010 system.

2.3. Photocatalysis

Photocatalysis experiments were performed in aqueous solutions containing TBP (A.R.) with an initial concentration of 0.1 mmol/L. The photocatalysis reactor consists of a 160 mL Pyrex glass chamber with a jacket outside and a 125 W high pressure Hg lamp in parallel to the Pyrex glass chamber. In all the experiments, the reaction temperature was kept at 27 ± 2 °C by a continuous circulation of water in the jacket around the reactor. Reaction suspensions were prepared by adding 0.225 g of M-TiO_2 photocatalyst powder into 150 mL TBP aqueous solution under vigorous stirring. Prior to irradiation, all reaction suspensions were stirred in the dark for 30 min to establish an adsorption–desorption equilibrium. A 3 mL sample solution was taken from the reactor at given time intervals, and filtered through a 0.2 μm millipore filter for analysis.

The concentrations of TBP in the suspensions were monitored by an Agilent 1200 high pressure liquid chromatography (HPLC) equipped with a UV detector (λ = 286 nm). After 50 μL samples were injected, the substances were separated by an Agilent C18 reverse-phase column (150 mm × 4.6 mm, 5 μm). The mobile phase consisted of 45 vol.% water and 55 vol.% acetonitrile pumped at 1 mL/min, and the column was thermostated at 35 °C. The chromatographic areas of experimental samples were converted to the concentration values using calibration curves based on the standard compounds.

3. Results and discussion

3.1. Morphological and structural characteristics of M-TiO_2

3.1.1. Effect of hydrothermal treatment

The wide angle XRD patterns of M-TiO_2 samples prepared with or without hydrothermal treatment are shown in Fig. 1. The XRD patterns obtained from samples with or without hydrothermal treatment exhibits similar characteristics, which can be indexed to 25.3 (1 0 1), 37.2 (0 0 4), 48.9 (2 0 0), 54.0 (1 0 5), 55.3 (2 1 1), 62.4 (2 0 4) and 68.7 (1 1 2), suggesting that anatase is the only crystalline phase in the sample [5]. The mean crystal sizes of the resultant M-TiO_2 were calculated from the broadening of the (1 0 1) XRD peaks of anatase phase according to the Scherrer formula [38]. The mean crystal sizes of 14.7 and 16.4 nm were obtained from samples with and without hydrothermal treatment, respectively.

Fig. 2 shows the N_2 adsorption/desorption isotherms and the Barrett–Joyner–Halenda (BJH) pore size distribution profiles (insert) of samples with and without hydrothermal treatment. All the profiles reveal a small hysteresis loop, implying the presence of mesopores at high relative pressure range between 0.4

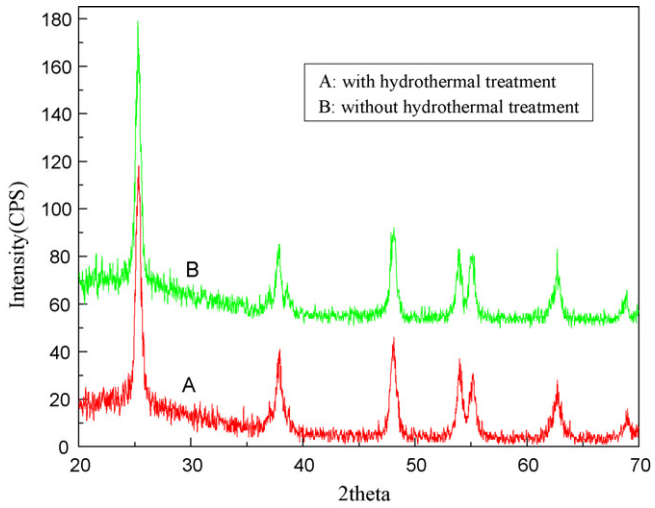

Fig. 1. XRD patterns of M-TiO_2 prepared with or without hydrothermal treatment.

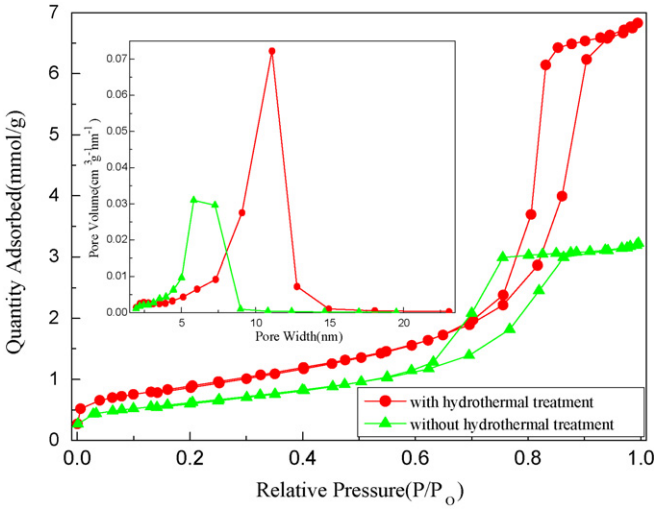

Fig. 2. N_2 adsorption/desorption isotherm and BJH pore size distribution of M-TiO_2 prepared with or without hydrothermal treatment.

and 0.8 (Type IV) [39]. Moreover, the N_2 adsorption quantity for the sample prepared with hydrothermal treatment is much higher than that of the sample without hydrothermal treatment, indicating the abundance of mesopores in a hydrothermally treated sample. The isotherm of hydrothermally treated sample exhibits a high Type IV adsorption/desorption shape with an H1 hysteresis loop, which implies that the synthesized M-TiO_2 samples consist of agglomerates or compacts of approximately uniform spheres in fairly regular array with a narrow range of pore size distribution [40,41]. However, for samples without hydrothermal treatment, the obtained isotherms display Type IV shape with a H2 hysteresis loop, suggesting the existence of ink-bottle pores with narrow necks and wide bodies [41]. The pore-size distribution profiles are given in the insert of Fig. 2. The maximum adsorption peaks valued at 11.1 and 6.4 nm were observed for samples with and without hydrothermal treatment, respectively. This suggests that the hydrothermal treatment can suppress the aggregation of the crystalline particles and can enlarge the pore size. The BET surface areas and other parameters were also investigated (see Table 1). Without hydrothermal treatment, the BET surface area of 50 m^2/g and the mean pore size of 6.3 nm were obtained. The BET surface areas and the mean pore size were increased to 72 m^2/g and 9.6 nm, respectively, when the sample was subjected to the hydrothermal treatment process. In addition, the microporous volumes observed for samples with and without hydrothermal treatment were 0.029 and 0.020 cm^3/g, respectively, but the total pore volumes observed for the hydrothermally treated sample (0.24 cm^3/g) was 200% greater than that observed for a sample without hydrothermal treatment (0.11 cm^3/g). This implies that the mesoporous structure of hydrothermally treated sample contains larger numbers of mesopores in comparison to the untreated sample.

3.1.2. Effect of PEG molecular weight

The effect of PEG molecular weight on the mean crystalline size of the hydrothermally treated sample was investigated. These hydrothermally treated samples were calcinated at 450 °C for 4 h. It was found that the mean crystalline sizes decreased from 17.0 to 13.3 nm when the molecular weight increased from 200 to 20,000 (see Table 2). This is in agreement with the work published by Devi et al. [5].

Fig. 3 shows the N_2 adsorption–desorption isotherms of hydrothermally treated M-TiO_2 samples prepared with different PEG molecular weights. All isotherms reveal Type IV curve characteristics with a small H1 hysteresis loop, indicating ordered cylindrical pores [40]. It was found that the amount of adsorbed N_2 increased significantly at certain molecular weight ranges. The lowest amount of adsorbed N_2 was observed with samples prepared with PEG molecular weights that ranged from 200 to 600. A sharp increase in the amount of adsorbed N_2 was recorded with samples prepared with PEG molecular weights that ranged from 1000 to 2000. When the molecular weight was increased to 20,000, a further increase in the amount of adsorbed N_2 was obtained. The effect of PEG molecular weight on the pore size distribution was also investigated (see the insert in Fig. 3). It was found that an increase in the PEG molecular weight leads to a stepwise increase in the pore size range and in the peak of the pore size distribution. For the PEG molecular weights of 200 and 600, the observed pore size distribution was ranged from 5.0 to 14.5 nm with a maximum adsorption peak at 11.0 nm. For the PEG molecular weights of 1000 and 2000, the observed pore size distribution ranged from 5.0 to 18.0 nm with a peak at 13.0 nm. A much broader pore size distribution was observed with the molecular weight of 20,000, which ranged from 5.0 to 22.5 nm

Table 1
Structural parameters of M-TiO_2 prepared with or without hydrothermal treatment

Pre-reaction condition	Crystalline size[a]	S_{BET}[b] (m^2/g)	Mean pore size[c]	Microporous volume[d] (cm^3/g)	Total volume[e] (cm^3/g)
Stir for 24 h and 48 h HT	14.7	72	9.6	0.029	0.24
Stir for 72 h	16.4	50	6.3	0.020	0.11

[a] Calculated by the Scherrer equation.
[b] BET surface area calculated from the linear part of the BET plot.
[c] Estimated using the desorption branch of the isotherm.
[d] Estimated by H-K method.
[e] Single-point total pore volume of pores at $P/P_0 = 0.99$.

Table 2
Structural parameters of M-TiO_2 prepared with PEG of different molecular weights

Molecular weight of PEG	Crystalline size[a]	S_{BET}[b] (m^2/g)	Mean pore size[c]	Microporous volume[d] (cm^3/g)	Total volume[e] (cm^3/g)
200	17.0	69	9.9	0.028	0.24
600	14.7	72	9.6	0.029	0.24
1,000	14.6	79	11.3	0.030	0.31
2,000	13.9	85	11.0	0.035	0.31
20,000	13.3	90	13.3	0.037	0.40

[a] Calculated by the Scherrer equation.
[b] BET surface area calculated from the linear part of the BET plot.
[c] Estimated using the desorption branch of the isotherm.
[d] Estimated by H-K method.
[e] Single-point total pore volume of pores at $P/P_0 = 0.99$.

with a peak at 15.0 nm. Interestingly, these stepwise increase trends caused by the PEG molecular size increase was also observed for the mean pore size and for the total volume (see Table 2).

3.1.3. Effect of calcination temperatures

The wide angle XRD patterns of hydrothermally treated M-TiO_2 calcinated at different temperatures were recorded (see Fig. 4). The anatase was found to be the only crystalline phase present in all samples, regardless of the treatment temperature. As expected, an increase in the treatment temperature results in an increase in the crystallinity. The mean crystalline sizes calculated from the XRD patterns using the Scherrer formula [38] were found to be increased from 9.8 to 36 nm when the treatment temperature was increased from 350 to 650 °C (see Table 3). The average particle sizes obtained from the present work are much larger than those in previously published data [6,21,24].

Fig. 5 shows the N_2 adsorption/desorption isotherms and pore size distribution profiles of hydrothermally treated M-TiO_2 calcinated at different temperatures. The characteristics of the recorded isotherms for all samples display a Type IV curve. A H1 hysteresis loop was observed for samples calcined at relatively low temperatures of 350, 450 or 550 °C. For the sample calcined at 650 °C, a H3 hysteresis loop from 0.6 to 0.99 relative pressure (P/P_0) was observed, indicating that aggregates of plate-like structures exist [41]. Fig. 5 also reveals that the amount of adsorbed N_2 decreased rapidly with increased calcination temperature. The isotherm obtained from the sample calcined at 650 °C indicates the amount of adsorbed N_2 was neglectable, which implies the completely collapsed mesoporous structure. The insert of Fig. 5 shows the pore size distribution profiles. It was found that, for the 350 °C-calcinated sample, the pore size distribution was peaked around at 9.1 nm with a substantial percentage of pores sized below 5.0 nm. For the 450 °C-calcinated sample, the distribution peak was shifted to around 11.1 nm with a neglectable percentage of pores sized below 5.0 nm. This could be due to the mesoporous structure consolidation as a result of improved crystallinity at higher calcination temperature. The pore size distribution profile obtained from the sample calcinated at 550 °C shows a peak around at 10.7 nm, due to the formation of larger pores. An almost flatted pore size distribution profile was observed for the sample calcinated at 650 °C, which confirms the completely collapsed mesoporous structure.

The effect of the sample calcination temperature on the BET surface areas and other properties were also investigated (see Table 3). It was found that a sample with low calcination temperature (i.e. 350 °C) possesses high BET surface areas (i.e. 142 m^2/g). The observed BET surface area was rapidly reduced to 49 m^2/g when the calcination temperature was increased to 550 °C. The BET surface area of 7 m^2/g was measured from the sample calcinated at 650 °C, which again confirms the complete collapsed mesoporous structure. The data shown in Table 3 also

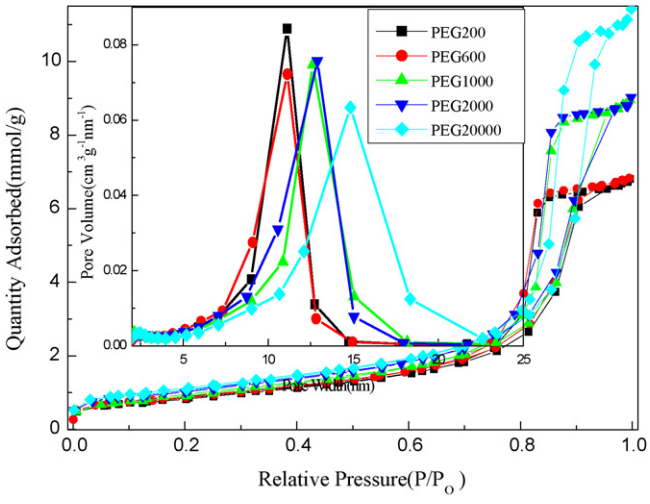

Fig. 3. N_2 adsorption/desorption isotherm and BJH pore size distribution of M-TiO_2 prepared with different molecular weights of PEG.

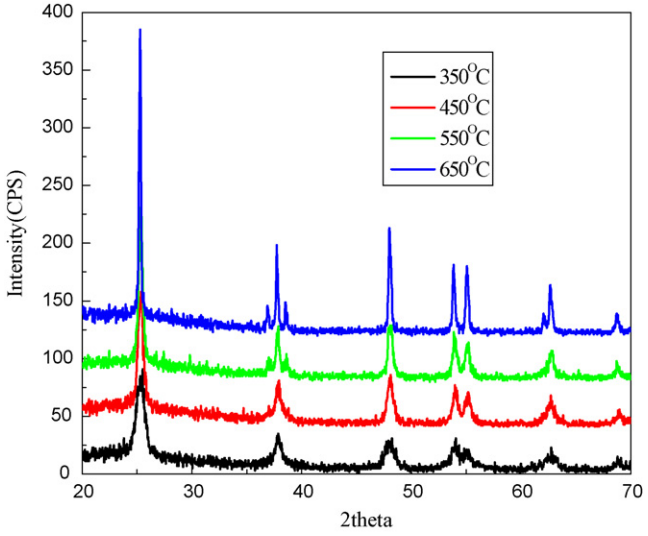

Fig. 4. XRD patterns of M-TiO_2 prepared with different calcination temperatures.

Table 3
Structural parameters of M-TiO_2 prepared under different calcination temperatures

Calcination temperatures (°C)	Crystalline size[a]	S_{BET}[b] (m^2/g)	Mean pore size[c]	Microporous volume[d] (cm^3/g)	Total volume[e] (cm^3/g)
350	9.8	142	8.0	0.057	0.38
450	14.7	72	9.6	0.029	0.24
550	18.4	49	10.0	0.020	0.18
650	36.0	7	15.8	0.003	0.05

[a] Calculated by the Scherrer equation.
[b] BET surface area calculated from the linear part of the BET plot.
[c] Estimated using the desorption branch of the isotherm.
[d] Estimated by H-K method.
[e] Single-point total pore volume of pores at $P/P_0 = 0.99$.

reveal that an increase in the calcination temperature from 350 to 650 °C leads to an increase in the mean pore sizes from 8.0 to 15.8 nm, and a decrease in both the microporous volume and the total volume. Though the largest mean pore size of 15.6 nm was observed from the sample calcinated at 650 °C, the neglectable microporous volume of 0.003 cm^3/g and the total volume of 0.05 cm^3/g suggest that the resultant material is nonporous, due to the collapsed mesoporous structure.

Fig. 6 shows the TEM images of samples calcined at 450 and 650 °C, respectively. The data show that, for the sample calcined at 450 °C, the obtained M-TiO_2 was formed by primary particles sized between 10 and 20 nm. Under such a calcination temperature, no secondary particle formation was observed (see Fig. 6a). For the sample calcined at 650 °C (see Fig. 6b), the primary particles can no longer be discerned. Under such conditions, the edges of primary particles in the secondary particles blurred to such an extent that they could not be easily recognized, due to a high degree of aggregation between primary particles. The formation of large size secondary particles and highly compacted packing of these secondary particles destroy the mesoporous structure, as evidenced by the above experimental data.

It should be mentioned that the images obtained from all samples before calcination (results are not shown) indicate that no aggregation occurred during the hydrolysis process and post hydrothermal treatment process. This may be due to the benefits of replacing strong acid with diluted acetic acid during the hydrolysis process. It is well known that the titanium precursor rapidly hydrolyzing in strong acid media often leads to the aggregation and formation of large size particles because of uncontrollable hydrolysis causes by the rapid pH change [27]. However, a hydrolysis media containing a weak acid such as acetic acid allows a better control of hydrolysis process [27]. In this process, acetic acid serves not just as a hydrolytic retardant but also as chelating and pH buffering agent, enabling a slower and uniform hydrolysis process.

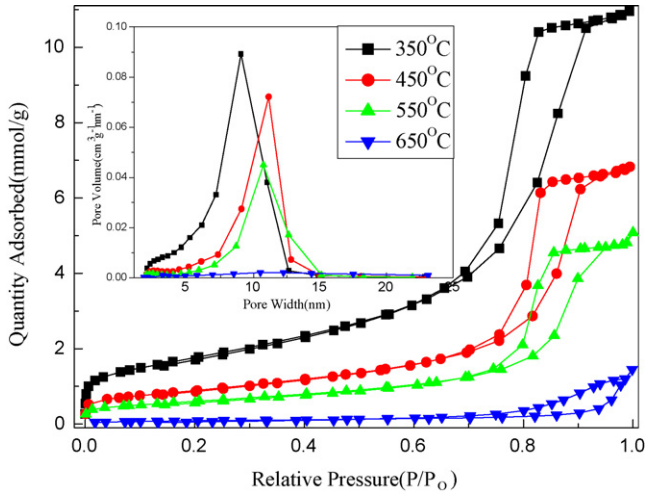

Fig. 5. N_2 adsorption/desorption isotherm and BJH pore size distribution of M-TiO_2 prepared with different calcination temperatures.

3.2. Photocatalytic degradation of TBP

Fig. 7 demonstrates the photolysis and photocatalytic degradation profiles of synthesized M-TiO_2 with or without hydrothermal treatment. Only less than 30% TBP can be decomposed in the photolytic process. Seen from the figure, M-TiO_2 prepared with hydrothermal treatment possesses exhibits significantly higher photocatalytic efficiency for the degradation of TBP than that of without hydrothermal treatment. After 60 min photocatalysis, a degradation efficiency of ca. 92.3% was acquired from hydrothermally treated M-TiO_2 photocatalyst while only 85.1% was obtained from M-TiO_2 prepared without hydrothermal treatment. This indicates that the hydrothermal treatment can improve not only the mesoporous structure and particles assembly, but also the photocatalytic degradation activity. The improved photocatalytic activity of M-TiO_2 synthesized with hydrothermal treatment may be attributed to the improved crystal phase composition/crystallinity, enhanced BET surface areas, high total volume and well-defined mesoporous structure [25].

The adsorption performances and the photocatalytic activity of mesoporous TiO_2 nanoparticles prepared with different molecular weight PEGs as structure-directing reagents was also compared, and the removal efficiencies of TBP are displayed in Fig. 8. The figure shows that both the adsorption and the degradation efficiencies of TBP increased with PEG molecular weight. The adsorption efficiencies increased from 5.32% to 6.26%, while the degradation efficiencies increased from 89.48% to 95.87% when PEG molecular weight was increased from 200 to 20,000. That is, the larger the PEG molecule, the higher of adsorption efficiencies of TBP and photocatalytic activity. The increase in the adsorptivity and photocatalytic efficiencies may be attributed to the decreased crystalline size of synthesized M-TiO_2 and the increased mesoporous parameters, such as the mean porous size, BET surface area and the total porous volume (see Table 2). The variations of the mesoporous structure parameter and the photocatalytic activity of synthesized M-TiO_2 may reflect some change in configuration of ethylene chain in the PEG matrix in accordance with the molecular weight of PEG [5]. When the molecular weight exceeds 400, the PEG chain may be twisted and the PEG segments could form crown-ether-type complexes with inorganic ions through weak coordination

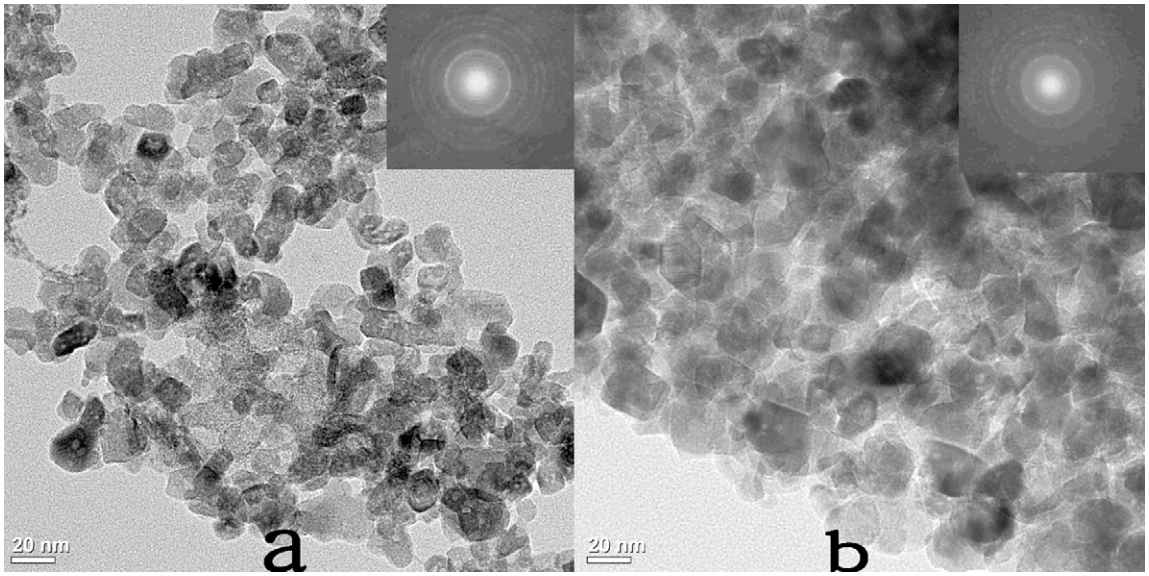

Fig. 6. TEM images of M-TiO_2 prepared with different calcination temperatures: (a) 450 °C and (b) 650 °C (the insert is the electron diffraction micro-image).

interactions [3,17]. During the aging process, PEG molecules lose their bonding water, producing free PEG molecules available to form tightly "particles-PEG" complexes [3]. Thus, a larger PEG molecule would result in a smaller crystalline size and larger mean porous size, BET areas and total volume, which, in turn, would lead to better adsorptivity and degradation efficiencies.

Fig. 9 shows the degradation profiles of TBP obtained from M-TiO_2 prepared at different thermal treatment temperatures. It was found that the TBP degradation efficiency increased as the sample calcination temperature increased from 350 to 550 °C and then sharply decreased when the sample calcination temperature further increased to 650 °C. The insert of Fig. 9 shows the rate constants of M-TiO_2 prepared at different thermal treatment temperatures. Pseudo-first-order degradation kinetics was observed, which is similar to the kinetics obtained from other mesoporous TiO_2 catalysis systems [42]. The TBP degradation rate constant was found to be rapidly increased from 0.010 to 0.018 min^{-1} when the thermal treatment temperature was increased from at 350 to 550 °C. A sharp decrease in the rate constant to 0.004 min^{-1} was observed from the sample thermally treated at 650 °C, indicating a sharp decrease in the photoactivity. As shown in Table 3, when the thermal treatment temperature increased from 350 to 550 °C, the resultant M-TiO_2 increased its crystalline size (representing the crystallinity) from 9.8 to 18.4 nm, while the BET areas decreased from 142 to 49 m^2/g. It is obvious that the increased crystallinity was the decisive factor for the increased photocatalytic degradation efficiency [43]. However, the low activity of 350 °C-calcined photocatalyst can be partly a result of the inhibiting effect of significant amounts of carbonaceous residues. On the contrary, the sharp decrease in the photocatalytic degradation efficiency obtained from the sample thermally treated under 650 °C was due to the completely collapsed mesoporous structure, as the data in Table 3 indicated.

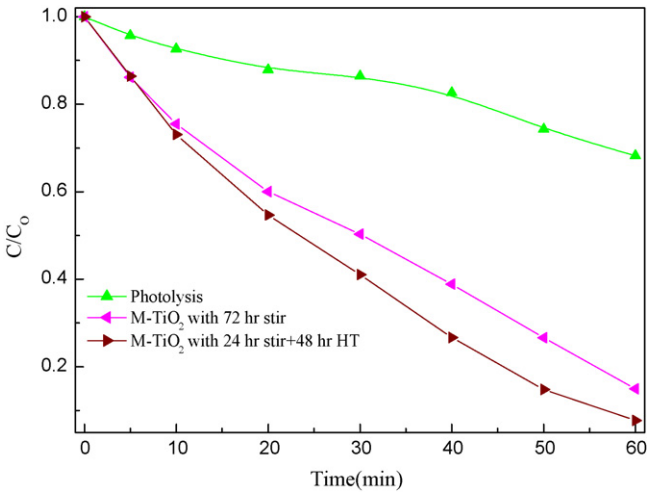

Fig. 7. Photocatalytic degradation curves with or without hydrothermal treatment compared with the photolysis.

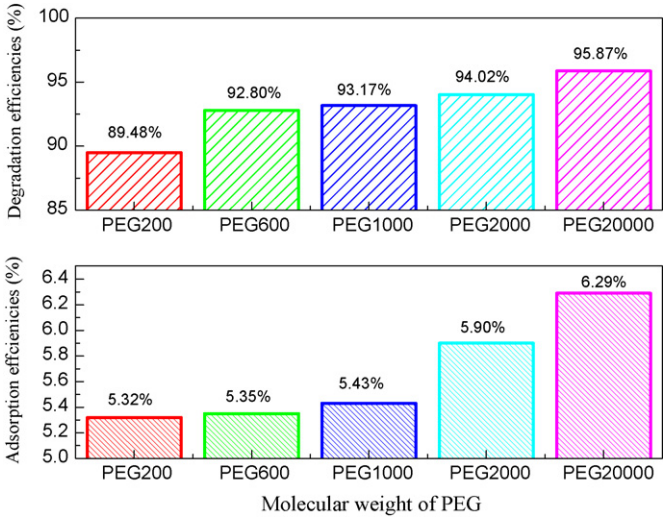

Fig. 8. Adsorption and photocatalytic efficiencies of TBP using M-TiO_2 photocatalysts prepared with different PEG molecular weights (the calcination temperature: 450 °C).

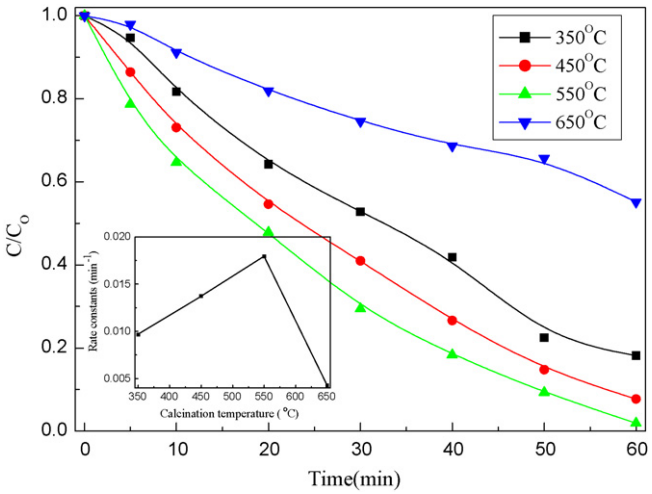

Fig. 9. Photocatalytic profiles of TBP using M-TiO_2 photocatalysts prepared with different calcination temperatures (the insert shows the first-order curves for the photocatalytic degradation of TBP).

Acknowledgements

This is contribution No. IS-1005 from GIGCAS. This work was financially supported by the National Natural Science Foundation of China (40572173 and 40632012) and the Science and Technology Project of Guangdong Province, China (2007A032301002 and 2006A36701002).

References

[1] C.T. Kresge, M.E. Leonowicz, W.J. Roth, J.C. Vartuli, J.S. Beck, Nature 359 (1992) 710–712.
[2] A. Taguchi, F. Schuth, Micropor. Mesopor. Mater. 77 (2005) 1–45.
[3] L. Zhang, Y. Zhu, Y. He, W. Li, H. Sun, Appl. Catal. B-Environ. 40 (2003) 287–292.
[4] H. Zhao, D. Jiang, S. Zhang, W. Wen, J. Catal. 250 (2007) 102–109.
[5] G.S. Devi, T. Hyodo, Y. Shimizu, M. Egashira, Sens. Actuators B-Chem. 87 (2002) 122–129.
[6] M.R. Mohammadi, D.J. Fray, M.C. Cordero-Cabrera, Sens. Actuators B-Chem. 124 (2007) 74–83.
[7] T. Dentani, K.I. Nagasaka, K. Funabiki, J.Y. Jin, T. Yoshida, H. Minoura, M. Matsui, Dyes Pigments 77 (2008) 59–69.
[8] P. Puhlfurb, A. Voigt, R. Weber, M. Morb, J. Membr. Sci. 174 (2000) 123–133.
[9] L. Yang, Y. Wang, D. Huang, G. Luo, Y. Dai, Ind. Eng. Chem. Res. 46 (2007) 579–583.
[10] Y. Chen, D.D. Dionysiou, Appl. Catal. A-Gen. 317 (2007) 129–137.
[11] R. Tan, Y. He, Y. Zhu, B. Xu, L. Cao, J. Mater. Sci. 38 (2003) 3973–3978.
[12] C. Wang, Z. Deng, Y. Li, Inorg. Chem. 40 (2001) 5210–5214.
[13] G.J.d.A.A. Soler-Illia, A. Louis, C. Sanchez, Chem. Mater. 14 (2002) 750–759.
[14] J.C. Yu, L. Zhang, J. Yu, New J. Chem. (2002) 416–420.
[15] K.S. Yoo, T.G. Lee, J. Kim, Micropor. Mesopor. Mater. 84 (2005) 211–217.
[16] C. Su, C.-M. Tseng, L.-F. Chen, B.-H. You, B.-C. Hsu, S.-S. Chen, Thin Solid Films 498 (2006) 259–265.
[17] J. Jiao, Q. Xu, L. Li, J. Colloid Interface Sci. 316 (2007) 596–603.
[18] H.X. Li, Z.F. Bian, J. Zhu, D.Q. Zhang, G.S. Li, Y.N. Huo, H. Li, Y.F. Lu, J. Am. Chem. Soc. 129 (2007) 8406–8407.
[19] D.M. Antonelli, J.Y. Ying, Angew. Chem. Int. Ed. Engl. 34 (1995) 2014–2017.
[20] J.F. Zhou, M.F. Zhou, R.A. Caruso, Langmuir 22 (2006) 3332–3336.
[21] H. Hirashima, H. Imai, V. Balek, J. Non-Cryst. Solids 285 (2001) 96–100.
[22] S.Y. Choi, M. Mamak, N. Coombs, N. Chopra, G.A. Ozin, Adv. Funct. Mater. 14 (2004) 335–344.
[23] J.K. Liu, T.C. An, G.Y. Li, X.Y. Zeng, N.Z. Bao, G.Y. Sheng, J.M. Fu, Micropor. Mesopor. Mater., submitted for publication.
[24] H. Sertchook, H. Elimelech, C. Makarov, R. Khalfin, Y. Cohen, M. Shuster, F. Babonneau, D. Avnir, J. Am. Chem. Soc. 129 (2007) 98–108.
[25] B. Wen, C. Liu, Y. Liu, J. Photochem. Photobiol. A-Chem. 173 (2005) 7–12.
[26] X.H. Hu, T.C. An, M.L. Zhang, G.Y. Sheng, J.M. Fu, Res. J. Chem. Environ. 11 (2007) 13–21.
[27] X.J. Ding, T.C. An, G.Y. Li, S.Q. Zhang, J.X. Chen, J.M. Yuan, H.J. Zhao, H. Chen, G.Y. Sheng, J.M. Fu, J. Colloid Interface Sci. 320 (2008) 501–507.
[28] L. Yang, Y. Wang, G. Luo, Y. Dai, Micropor. Mesopor. Mater. 94 (2006) 269–276.
[29] S.-R. Zhai, C.-S. Ha, Micropor. Mesopor. Mater. 102 (2007) 212–222.
[30] S.R. Zhai, C.S. He, D. Wu, Y.H. Sun, J. Non-Cryst. Solids 353 (2007) 1606–1611.
[31] K. Yu, J. Zhao, X. Zhao, X. Ding, Y. Zhu, Z. Wang, Mater. Lett. 59 (2005) 2676–2679.
[32] Y. Saito, S. Kambe, T. Kitamura, Y. Wada, S. Yanagida, Sol. Energy Mater. Sol. Cells 83 (2004) 1–13.
[33] M. Nichkova, M. Germani, M.P. Marco, J. Agric. Food Chem. 56 (2008) 29–34.
[34] A. Bergman, Brominated Flame Retardants in a Global Environmental Perspective, National Chemicals Inspectorate, Skokloster, Solna, 1990.
[35] F.B. Whitfield, J.L. Hill, K.J. Shaw, J. Agric. Food Chem. 45 (1997) 889–893.
[36] M. Gutierrez, J. Becerra, J. Godoy, R. Barra, Int. J. Environ. Health Res. 15 (2005) 171–179.
[37] J.W. Blythe, A. Heitz, C.A. Joll, R.I. Kagi, J. Chromatogr. A 1102 (2006) 73–83.
[38] H.P. Klug, L.E. Alexander (Eds.), X-ray Diffraction Procedures for Polycrystalline and Amorphous Materials, Wiley, New York, 1974.
[39] J.G. Yu, L.J. Zhang, B. Cheng, Y.R. Su, J. Phys. Chem. C 111 (2007) 10582–10589.
[40] M. Kruk, M. Jaroniec, Chem. Mater. 13 (2001) 3169–3183.
[41] K.S.W. Sing, D.H. Everett, R.A.W. Haul, L. Moscou, R.A. Pierotti, J. Rouquerol, T. Siemieniewska, Pure Appl. Chem. 57 (1985) 603–619.
[42] T.C. An, X.H. Zhu, Y. Xiong, Chemosphere 46 (2002) 897–903.
[43] J.C. Yu, J. Yu, L. Zhang, W. Ho, J. Photochem. Photobiol. A-Chem. 148 (2002) 263–271.